Transactions, **SMiRT-26**
Berlin/Potsdam, Germany, July 10-15, 2022
Division Special Session

SIMULATION OF PRE-STRESSED SLABS USING ABAQUS CDP MATERIAL MODEL

Kubilay Özen[1] and Alexis Fedoroff[2]

[1] Structural Engineer, AFRY, Jaakonkatu 3, 01620 Vantaa, Finland (kubilay.ozen@afry.com)
[2] Senior Scientist, VTT, Kemistintie 3, Espoo, Finland (alexis.fedoroff@vtt.fi)

ABSTRACT

In this study, appropriate methodology and finite element models have been developed in order to simulate hard impact on reinforced and pre-stressed concrete slabs. The developed models were validated by the impact tests reported by VTT. The tests included the collision of approximately 47 kg missiles, having impact velocities around 120 m/s, on reinforced and pre-stressed concrete square slabs (2.1 x 2.1 x 0.25 m). Three threshold parameters of the element removal algorithm have been used to calibrate the FE models. The residual velocities and the ultimate capacities of the slabs have been compared with the experimental study, which were in good agreement.

INTRODUCTION

Accurate simulation of hard projectile impact on reinforced or pre-stressed concrete has proven to be a difficult task. For practical design purposes, the use of empirical formula is often sufficient for a conservative structural dimensioning. However, if the task is to obtain an accurate computational response that matches experimentally observed results, then empirical formulas and even most off-the-shelf material models readily available in commercial FEM software fail to produce consistently satisfactory results. One possible strategy is to use either user subroutines, (Fedoroff, et al., 2017), (Fedoroff & Calonius, 2020), in order to modify some of the constitutive behavior of the off-the-shelf model or to write new material subroutines from scratch, (Vilppo, et al., 2021). In both cases, the aim is to program a constitutive behavior that induces more accurate responses in hard projectile impact simulations. In particular, a correct handling of the material triaxial behavior and adequate fragmentation algorithms are key to success.

The actual concrete model under consideration is the Concrete Damaged Plasticity (CDP) model available in the Abaqus FE software with appropriate modifications applied via the user-defined-field-variable subroutine (VUSDFLD). The modifications consist of additional confinement dependency of isotropic hardening/softening behavior in uniaxial compression, strain rate dependency of isotropic softening behavior in uniaxial tension as well as an element removal algorithm based on a condition on shear strain measure together with a condition on triaxial confinement. The exact description of the user modified model can be found in (Fedoroff, et al., 2019) and (Fedoroff & Calonius, 2020). The objective is first to calibrate the physical model parameters using material test data provided from various compressive, tensile and triaxial concrete tests, (Calonius, et al., 2019), and subsequently to carry out a sensitivity study of internal model parameters that can't be calibrated from material tests. Experimental benchmark tests responses are used as reference. The experimental benchmark case chosen in this work consists of three reinforced concrete slabs, one without pre-stressing tendons, the second with pre-stressing tendons with zero applied tension, and the third with pre-stressing tendons with applied tension of 820 MPa. The detailed test description can be found in (Orbovic, et al., 2015).

There are three internal model parameters that this study is focusing on. The first is the shear strain threshold. The second parameter is the confinement stress. Both the strain threshold and the confinement stress threshold values affect the element removal algorithm. The third is the choice of weight coefficients for the computation of the confinement stress at each integration point. The weight coefficient determines the importance of current stress state as opposed to the time-maximum stress state in the computation of the confinement stress. It has been shown in previous studies, (Fedoroff, et al., 2019), that these parameters have influence on the simulation response. A parameter value grid of 3x3x3 has been chosen in this study to carry out the sensitivity analysis. The response values that are monitored and compared to the experimental results are the residual velocity or penetration depth as well as the overall failure mode of the slab.

DESCRIPTION OF THE USER MODIFIED ABAQUS CDP CONCRETE MODEL

Yield Surface and Flow Rule

The capability of built-in Abaqus CDP model was further enhanced by Fedoroff (2017) and Fedoroff et al. (2019), developing the User Modified CDP for the simulation of hard impact on concrete. The effects of confinement and strain rate on concrete subjected to collision was described and included in the CDP model by introducing a compressive hardening/softening behavior depending on confining stresses and tensile softening behavior depending on strain rates (Fedoroff et al., 2019). Furthermore, an element removal algorithm based on the pure-shear-strain state was developed. This algorithm was implemented through a VUSDFLD subroutine. The adopted user modified CDP model excludes the damage evolution differing from the built-in CDP model since the cyclic loading action may be neglected in hard impact scenarios on concrete. The user modified model uses the same yield surface as in the standard CDP model (Fedoroff, 2017),

$$f(\boldsymbol{\sigma}, \sigma_c, \sigma_t) = \frac{1}{1-a}\left(\tilde{q} + 3a\tilde{p} + \left(\frac{\tilde{\sigma}_c}{\tilde{\sigma}_t}(1-a) - (1+a)\right)\langle\tilde{\sigma}_{max}\rangle - \gamma\langle-\tilde{\sigma}_{max}\rangle\right) - \tilde{\sigma}_c, \tag{1}$$

where $\boldsymbol{\sigma}$ is the stress tensor, σ_c is the compressive cohesion stress, σ_t is the tensile cohesion stress, a as well as γ are the CDP model parameters, $\tilde{q}$ is the equivalent Mises stress, $\tilde{p}$ is the effective hydrostatic pressure, $\tilde{\sigma}_c$ is the effective compressive cohesion stress, $\tilde{\sigma}_t$ is the effective tensile cohesion stress, and $\tilde{\sigma}_{max}$ is the equivalent maximum principal stress. The cohesion stress in compression, depends on the confinement stress, $\tilde{\sigma}_{cnf}$, whereas the cohesion stress in tension depends on the maximum principal strain rate. The consistency condition can be utilized to obtain the plastic flow coefficient, before using the flow rule to calculate uniaxial-tensile, uniaxial-compressive, and pure-shear-strain-state plastic strain increments (Fedoroff et al., 2019).

The change in hardening/softening variables are defined with the use of a hyperbolic Drucker-Prager function as in the built-in CDP model. The ductility of concrete is greatly influenced by the dilation angle (θ). At the angles approximately at 56.3˚, concrete shows a high ductile response (Malm, 2006). For this reason, it is preferable to select lower dilation angle values, to capture the quasi-brittle behavior of concrete. The plastic flow potential function, where e is the eccentricity and σ_{t0} is the initial tensile yield stress, can be shown as below (Abaqus Manual, 2016):

$$g(\tilde{\boldsymbol{\sigma}}) = \sqrt{\tilde{q}^2 + (\sigma_{t0} e \tan\theta)^2} + \tan\theta\, \tilde{p}. \tag{2}$$

Element Deletion Algorithm

The removal of excessively distorted elements is essential for the realistic modeling of concrete structures undergoing fragmentation due to impact by penetrating or perforating projectiles. Otherwise, the extreme

deformation of elements may result in disruption of the ongoing simulation. Element deletion algorithms are introduced with threshold criteria that need to be determined.

The User Modified CDP model adopts an element deletion mechanism depending on the "cutoff shear strain" in the pure-shear-strain state (Fedoroff et al., 2019). The choice of the pure-shear-strain state as a basis for element removal is motivated by the fact that in hard impacts both tunneling and shear cone formation occur along a localized (mode II) shear zone. Delamination at the back face of the target wall, on the other hand, occurs mainly along a localized tensile (mode I) zone.

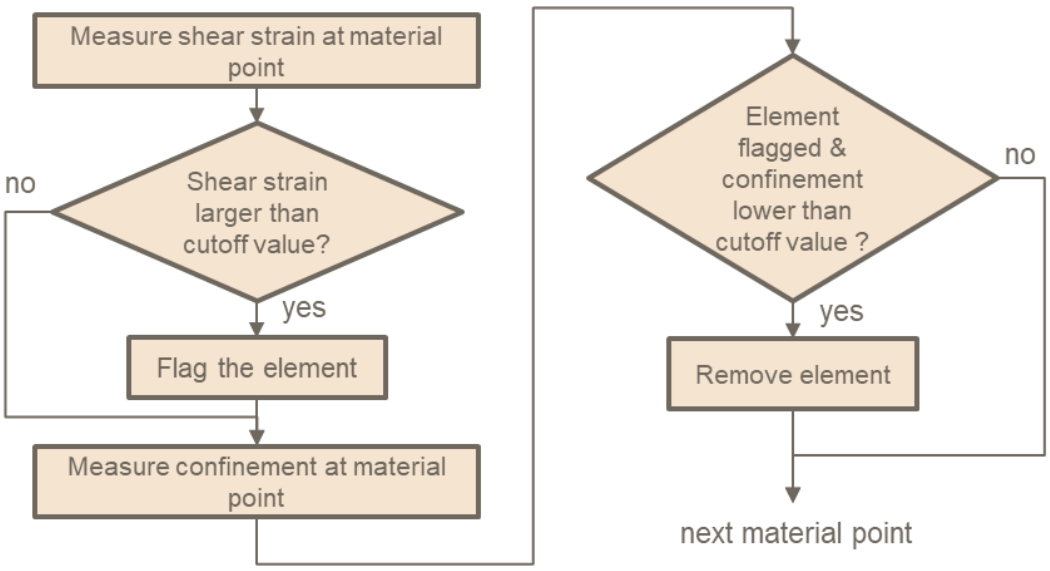

Figure 1. Flowchart for element deletion algorithm (Özen, 2021).

The VUSDFLD subroutine defines the deletion algorithm, which calls material point data from Abaqus Explicit at each time step. The input is then computed by the subroutine to determine where the loaded element is in state of removal. A flag variable, among other state variables used for extracting supplementary data to monitor the simulation, initiates the removal of the element (Özen, 2021).

The subroutine computes the confinement ratio (CR), using an arbitrary weight function to restrain the irregular variation of confinement stresses at consecutive time steps as

$$\mathrm{CR}(t) = (\omega_1 \tilde{\sigma}_{cnf}(t) + \omega_2 \tilde{\sigma}_{cnf}^{max}(t))/f_{cm}, \tag{3}$$

where $\tilde{\sigma}_{cnf}(t)$ is the current computed confinement stress at time t, f_{cm} concrete's compressive mean strength, and $\tilde{\sigma}_{cnf}^{max}(t)$ is the maximum effective confinement stress in the entire simulation run up to time frame t (Fedoroff and Calonius, 2020). The Equation 3 shows the weight coefficients ($\omega_1 + \omega_2 = 1.0$), which are used in a parametric study presented in the following sections to calibrate the algorithm. If the strains in pure-shear-strain state (ε_{psh}) surpasses the limiting cutoff shear strain ($\varepsilon_{max}^{cutoff}$), the distorted element is deleted from the simulation (Fedoroff and Calonius, 2020),

$$\varepsilon_{psh} \geq \varepsilon_{max}^{cutoff} \mathrm{P}_{psh}. \tag{4}$$

Additionally, a new threshold parameter (P_{psh}) for pure-shear-strain state is introduced to calibrate the maximum cutoff value, which helps to adjust the perforation strength of the structure under impact (Özen, 2021). The dependency on the mesh size is eliminated by calibrating the parameter ($\Gamma_{psh} = \frac{l_{min}}{20}$) (Fedoroff and Calonius, 2020), depending on the initial minimum characteristic length (l_{min}). The variable ($\varepsilon_{psh} = \delta\varepsilon_{oct}\Gamma_{psh}$) can be given in terms of the octahedral strains ($\varepsilon_{oct} = \varepsilon/\sqrt{2}$) dependable on the strain tensor (ε) in pure-shear-strain conditions (Fedoroff and Calonius, 2020). With the inclusion of three principal strains ($\varepsilon_{min}, \varepsilon_{mid}, \varepsilon_{max}$), the variable δ differentiates the strain conditions having high octahedral strains from the pure-shear-strain conditions, and it is shown with Expression 5 (Fedoroff and Calonius, 2020),

$$\delta = H(\varepsilon_{max})\left\langle 1 - \frac{\sqrt{\left(\varepsilon_{mid}+\frac{1}{2}\varepsilon_{max}\right)^2+\left(\varepsilon_{min}+\frac{1}{2}\varepsilon_{max}\right)^2}}{\sqrt{(\varepsilon_{max})^2+(\varepsilon_{mid})^2+(\varepsilon_{min})^2}}\right\rangle, \tag{5}$$

where the Heaviside operator is defined as $H(x) = \frac{1}{2}(sign(x) + 1)$, and the Macaulay bracket as $\langle x \rangle = \max(x, 0)$.

Another crucial mechanism for the element removal algorithm is to prevent the premature and improper deletion of the elements that have adequate confinement. This limit is obtained with the introduction of the confinement threshold parameter (P_{conf}) and Inequality 6 (Fedoroff and Calonius, 2020; Özen, 2021),

$$\tilde{\sigma}_{cnf} \leq 1.235 f_{cm} P_{conf}. \tag{6}$$

This study involves a parametric study on the threshold parameters (P_{conf}, P_{psh}) and weight coefficients (ω_1/ω_2) to calibrate the residual velocities of missiles in the FE models according to the tested specimens. When P_{conf} is set to lower values, lower values of the confinement stress prevent the algorithm from removing the element. When P_{psh} is adjusted to higher values, the algorithm does not allow the deletion of the element for higher pure-shear-strain-state strains.

DESCRIPTION OF THE BENCHMARK MODEL

The experimental study by Orbovic et al. (2015) at VTT, Technical Research Centre in Finland, on three hard-impacted concrete slabs investigated the influence of pre-stressing and the perforation capacities of the slabs. The missile impact velocities were 120.2, 120.5, and 117.9 m/s for specimens K, L and M, respectively.

Three 250 mm thick square specimens (2.1 m X 2.1 m) were supported with a 2 m span and reinforced with 10 mm steel bars, having 500 MPa of yield strength. While the specimens had identical longitudinal bars horizontally spaced at 90 mm in each way and on both faces with a concrete cover of 20 mm, specimens L and M had additional anchorage bars for locally introduced stresses due to pre-stressing. Slabs K, L, and M had cylinder mean compressive strengths of 53.4, 48.4, and 51.2 MPa, respectively. High-strength Dywidag bars, which were 26.5 mm and 548 mm^2 in diameter and area, respectively, were used to pre-stress the concrete slabs. The high-strength bars, with an ultimate strength of 1030 MPa, were equally spaced in PVC sleeves at 180 mm in both directions. The bars were pre-stressed to 820 MPa in order to achieve 10 MPa of confining stresses within the slabs.

Hard impact on concrete slabs were obtained by rigid missiles, which were steel covered and filled with lightweight concrete. The 168.3 mm in diameter and 640 mm long missiles had a steel cover of 10 mm. The impacting projectiles had masses of 47 kg approximately (Sagals et al., 2015).

FINITE ELEMENT MODELING

Abaqus Explicit is utilized to develop the three-dimensional models of the tested slabs. Mesh sizes are chosen according to the suggestion by Thai and Kim (2017), which is 11 mm. The eight-node C3D8R elements is chosen for the discretization of the concrete slabs and pre-stressing bars, to improve the contact mechanism, whereas linear beam elements are adopted for the embedded reinforcement (Figures 2 and 3). For shorter simulation runs, quarter modeling technique is used and support as well as anchoring plates are discretized with rigid elements, for specimens L and M. Contact surfaces within the concrete elements, and between the interior concrete surface and tendon duct are defined separately, to capture the realistic response of the perforating missile.

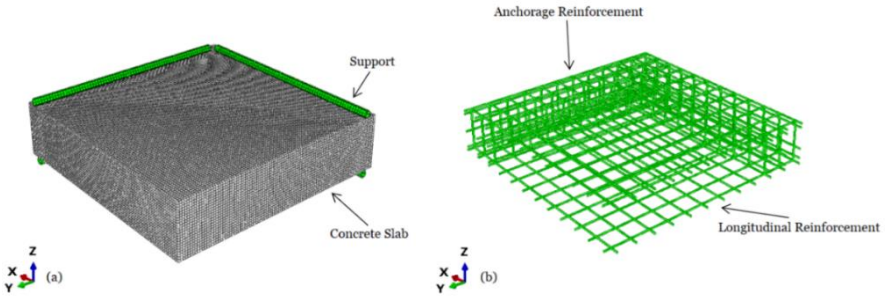

Figure 2. Concrete model (a), reinforcement model (b).

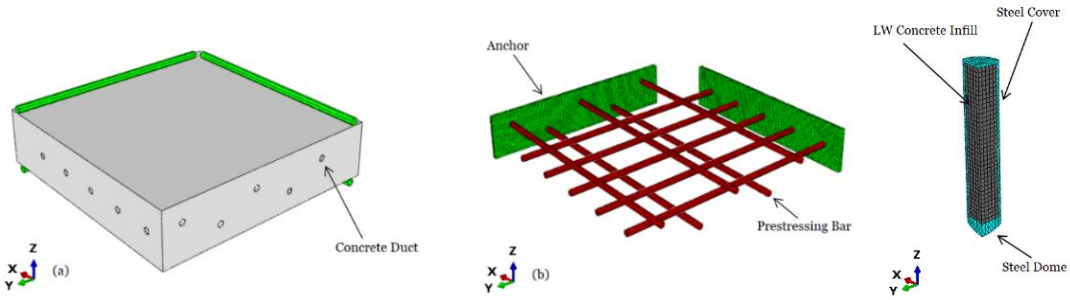

Figure 3. Prestressed concrete slab model (a), anchor and pre-stressing bar (b), missile model on far right.

The same C3D8R elements are used in missile modeling, which shared common mesh nodes at the contact surfaces, to improve computational performance and simulate welding as well as steel concrete bond. While initial missile velocities for specimens K and L were assigned to the missiles, the missile was placed at a distance with an initial acceleration to complete the pre-stressing step for specimen M.

Application of Pre-stressing

Various approaches have been preferred for the introduction of pre-stressing in concrete (Thai and Kim, 2017; Rajput et al., 2018). This study adopts the temperature loading method to shorten the Dywidag bars, thus applying post-tensioning stresses to the specimens as suggested by Ren et al. (2014).

The change in temperature required to achieve the compressive stresses in the slabs is calculated as follows (Ren et al., 2014);

$$T = -P/(cE_sA_{ps}), \tag{7}$$

where c is the thermal-expansion coefficient, P is the pre-stressing force, and E_s is the elastic moduli of the bars with an area of A_{ps}. The efficient time step for post- tensioning is found be 0.01 s.

Material Input Data

In the model, grade C45/55 concrete is used in the specimen K, while grade C 40/50 concrete is preferred for slabs L and M. The concrete hardening/softening behavior of C40/50 in both compression and tension is presented in Figure 4. The compressive and tensile stress evolution of C45/55 concrete is given in Figure 5.

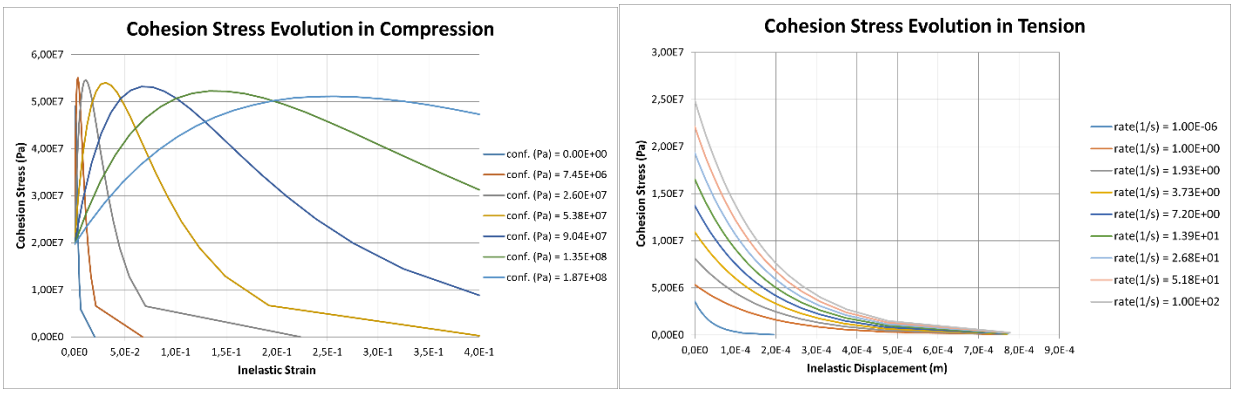

Figure 4. C40/50 concrete cohesion stress evolution in compression (left), tension (right).

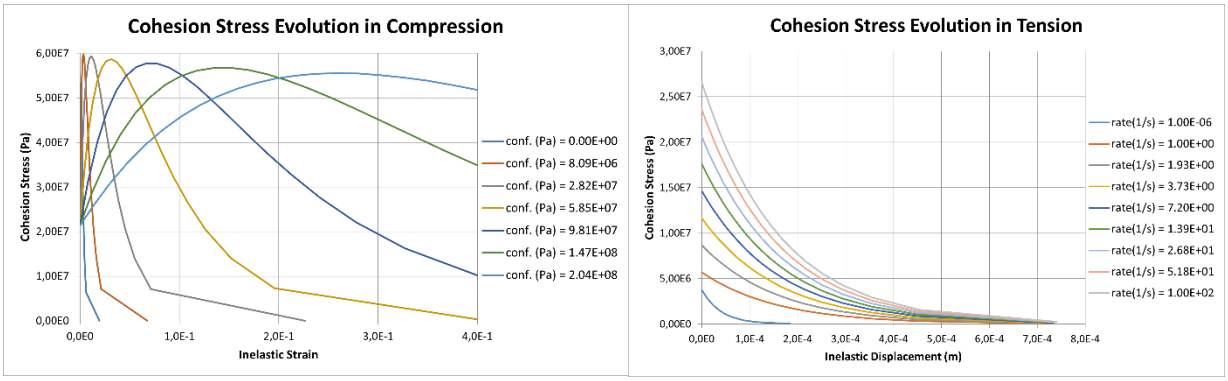

Figure 5. C45/55 concrete cohesion stress evolution in compression (left), tension (right).

The reinforcement behavior is specified with Mises's plasticity with Johnson-Cook damage definition. Finally, Orbovic et al. (2015) reported that the pre-stressing bars did not rupture in overall during the experimental study. Although there were some local plastic deformations in specimen L, no plastic

deformation was observed in specimen M. These findings have led to adoption of linear elastic material model in this study.

RESULTS

Parametric Study on Element Deletion Algorithm

To simulate hard impact scenarios on reinforced and pre-stressed concrete structures, this study aimed to find the most favorable set of parameters. In total, 81 simulations took place on two weight coefficients (ω_1/ω_2), P_{psh}, and P_{conf}. Different values for these parameters are presented in Table 1.

Table 1: Weight coefficients and threshold parameters.

ω_1/ω_2	0.6/0.4	0.5/0.5	0.4/0.6
P_{psh}	1.25	1.50	1.75
P_{conf}	0.40	0.50	0.60

The parametric study's results are presented in Table 2, where "Mm" is the missile mass. The best set of parameters is chosen to be $P_{conf} = 0.4, P_{psh} = 1.5,$ as well as $\omega_1/\omega_2 = 0.5/0.5$ and highlighted with yellow. If the collided missile rebounds after the impact the sign of the value is negative. The outcome of this study indicated that specimens L and M were more sensitive to the threshold parameters. One cause of this behavior could be the arising confinement stresses in elements between the projectile and pre-stressing bars (Özen, 2021).

Table 2: Residual velocities for different combinations

Specimen	ω_1/ω_2	0.6/0.4, Mm=47.2kg			0.5/0.5, Mm=47.4kg			0.4/0.6, Mm=47.4kg		
	P_{psh} \ P_{conf}	0.4	0.5	0.6	0.4	0.5	0.6	0.4	0.5	0.6
K	1.25	48	51	50	48	49	50	38	46	48
	1.50	44	48	50	42	47	48	40	43	45
	1.75	40	42	47	41	43	45	38	40	42
L	1.25	35	34	37	30	32	32	22	25	26
	1.50	28	32	28	22	24	28	13	18	24
	1.75	24	25	29	-8	20	25	6	6	13
M	1.25	21	29	31	-1	19	26	-1	2	19
	1.50	17	22	19	-6	9	17	-9	-12	-1
	1.75	-11	11	19	-8	-13	-2	-4	-8	-12

FE Results of Modeled Specimens

Overall, the prominent failure mode was punching failure as a result of the observation in all the specimens. A concrete plug was also formed in the specimens after the hard impact. The simulations showed that the FE results were more conservative on estimating the cone angle of the deformation, being steeper than the test results (Figure 6). Decreasing of cone angles for specimens L and M compared to the slab K was in parallel with the experimental findings.

Considering that the Figure 6 is not representing the scabbed area but the actual concrete plug formation, the results of the models were similar to the ones of the experimental study. The actual concrete part coming out after the collision in the FE models is highly comparable to the tested specimens.

Rupturing and elongating steel reinforcements existed in all specimens. The deformation of the simulated reinforcing steel bars on the distal and proximal faces were found to be resembling the actual cases.

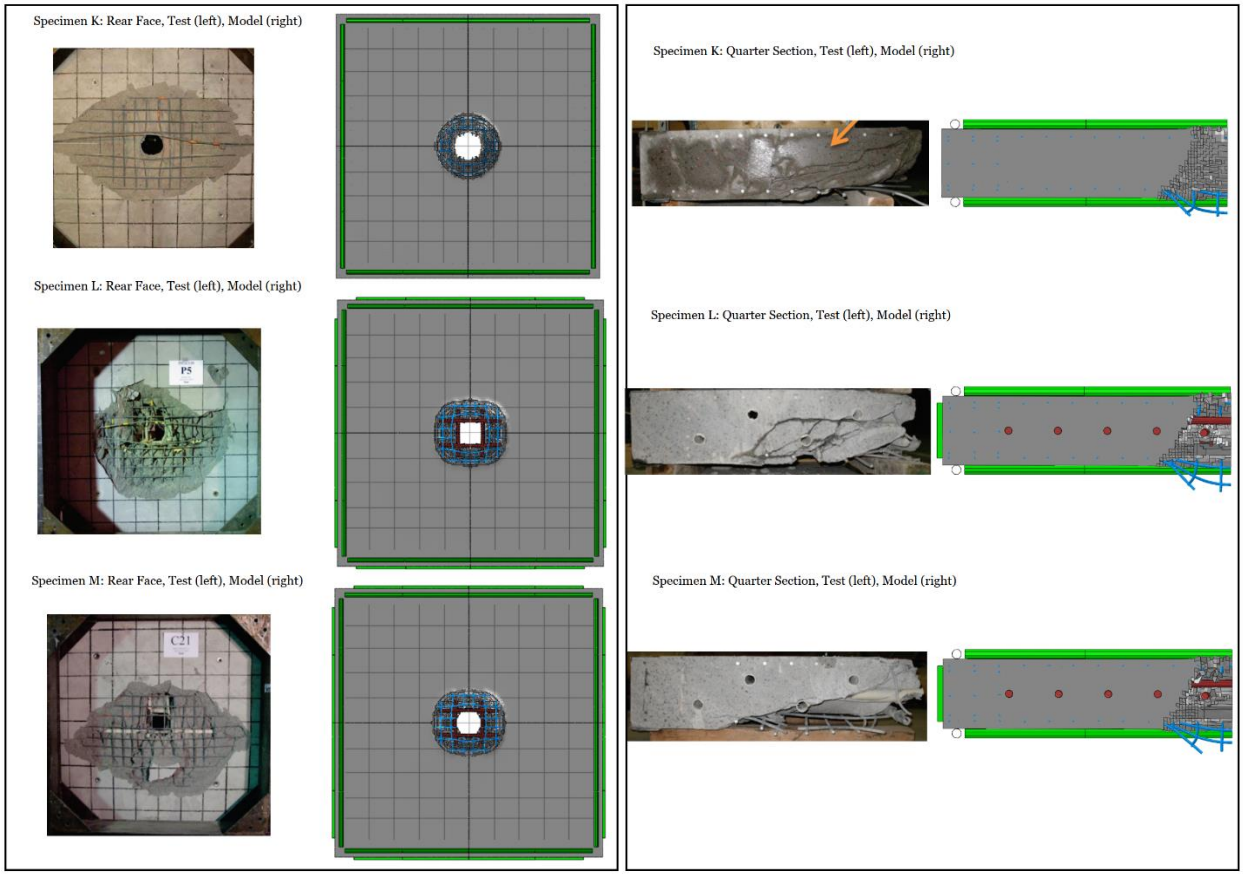

Figure 6. Comparisons of specimens after impact, rear view (left), section view (right).

Missile Residual Velocities

The main goal of this study was to estimate residual velocities of impacting missiles on reinforced and prestressed concrete structures, in addition to the structure's perforation capacities. Final residual velocities with the most optimal set of threshold parameters are given in Table 2.

While the specimen K had a residual velocity of 42 m/s, which is 27% higher than the experimental data at 33 m/s, slab L had a final velocity of 22 m/s, being 27% slower than the tested slab at 30 m/s. Notice also that in experimental tests, due to small variations in impact velocities between tests and due to inaccuracies in the determination of the experimental residual velocity, the error range can be as high as ±5m/s.

In specimen M, the experimental study showed that the missile was not able to penetrate through the slab and the final missile velocity was unavailable. This finding was similar to FE results of slab M, where the pre-stressed concrete prevented the perforation of the colliding missile (Figure 7). Additionally,

this study excluded the investigation of the main cause of such behavior. Sagals et al. (2015) questioned this behavior and found that prestressed Dywidag bars had a substantial effect on the ultimate perforation capacity of the concrete slabs.

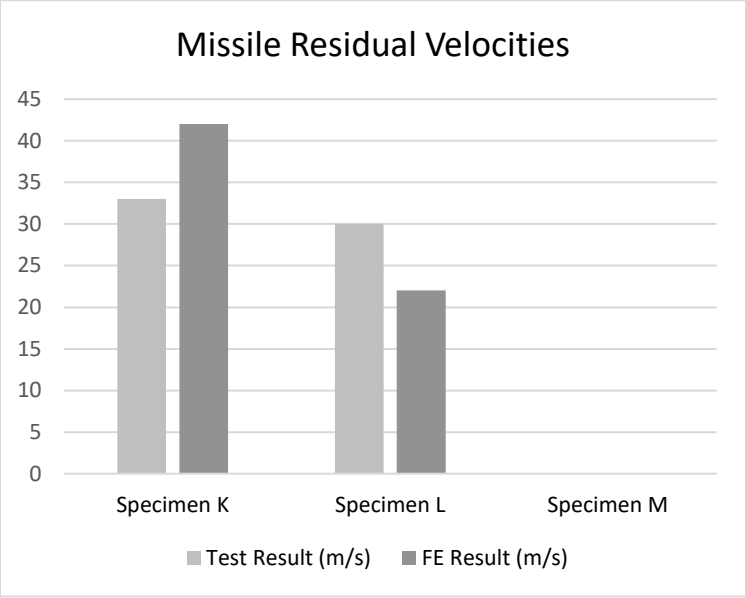

Figure 7. Comparison of missile residual velocities.

CONCLUSION

Distinct physical properties of the simulated slabs gave rise to the complexities in the FE modeling. These complexities included the existence of pre-stressing stresses and bars. This study dealt with such difficulties to accurately foresee the concrete slabs' ultimate perforation strengths and missile residual velocities.

The performance of the element removal algorithm was satisfactory in capturing the residual velocities of impacting missiles after the collision. Although the amount of scabbing was not compared with the test results, the intensity of concrete plug formation was similar to the experimental data. The cone angle after impact tended to be higher for FE models than the tests. For these reasons, it can be said the User Modified CDP model with introduced threshold parameters was highly capable of assessing the perforation capacity of reinforced and prestressed concrete slabs under impact and missile residual velocities.

A linear-elastic material model was used for modeling pre-stressing bars. This material model performed well during the FE analysis in this study. However, this material behavior can be enhanced by implementing an elastic-plastic material model with rate dependency. An experimental study can be conducted to investigate the strain-rate effects of the pre-stressing bars to be used in the development of such model.

REFERENCES

Abaqus Manual (2016). *User's Manual*. Dassault Systemes Simulia, Inc.

Fedoroff, A. (2017). "Continuum damage plasticity for concrete modelling," VTT Research Report, VTT-R-00331-17.

Fedoroff, A., & Calonius, K. (2020). "Using the Abaqus CDP model in impact simulations," *Rakenteiden Mekaniikka*, 53(3), 180-207. doi: 10.23998/rm.79723

Fedoroff, A., Calonius, K., & Kuutti, J. (2019). "Behavior of the Abaqus CDP model in simple stress states," *Journal of Structural Mechanics*," 52(2), 87-113. doi: doi.org/10.23998/rm.75937

Malm, R. (2006). "Shear cracks in concrete structures subjected to in-plane stresses," thesis, KTH Royal Institute of Technology.

Orbovic, N., Galan, M., & Blahoainu, A. (2015). "Hard missile impact tests in order to as-sess the effect of pre-stressing on perforation capacity of concrete slabs," *In Transactions of 23rd SMiRT*, Manchester, United Kingdom, August.

Özen, K. (2021). "Finite element analysis of prestressed concrete slabs under impact loading," Master's thesis, Aalto University School of Engineering. http://urn.fi/URN:NBN:fi:aalto-2021121910899

Rajput, A., Iqbal, M. A., & Wu, C. (2018). "Prestressed concrete targets under high rate of loading," *International Journal of Protective Structures*, 9(3), 362-376. doi: 10.1177/2041419618763933

Ren, W., Sneed, L. H., Yang, Y., & He, R. (2015). "Numerical simulation of prestressed pre-cast concrete bridge deck panels using damage plasticity model," *International Journal of Concrete Structures and Materials*, 9(1), 45-54. doi: 10.1007/s40069-014-0091-2

Sagals, G., Orbovic, N., & Blahoianu, A. (2015). "Numerical simulation of missile impact on reinforced concrete slabs: Effect of concrete pre-stressing," *In Transactions of 23rd SMiRT* doi: 10.13140/RG.2.1.2285.2323

Thai, D., & Kim, S. (2017). "Numerical simulation of pre-stressed concrete slab subjected to moderate velocity impact loading," *Engineering Failure Analysis*, 79 doi: 10.1016/j.engfailanal.2017.05.020

Vilppo, J., Kouhia, R., Hartikainen, J., Kolari, K., Fedoroff, A., & Calonius, K. (2021). "Anisotropic damage model for concrete and other quasi-brittle materials," *Internation Journal of Solids and Structures*, 225.